Pt−Sn Microfabricated Surfaces as Catalysts for Organic Electro-oxidation

María J. González,[†] Christopher H. Peters,[‡] and Mark S. Wrighton*

Department of Chemistry, Massachusetts Institute of Technology, Cambridge, Massachusetts 02139

Received: December 18, 2000; In Final Form: March 16, 2001

Microfabrication techniques have been used to prepare electrode surfaces reproducibly with well-defined composition and active area. Characterization of surfaces thus prepared leads to straightforward composition−activity and structure−activity relations. Conventional e^- beam deposition/lift-off techniques were used to fabricate the catalysts from a photopatterned resist on Pt. Catalysts consist of an array of closely spaced microstructures (circles or squares, 0.1 μm thick, 10−200 μm wide) of Sn on Pt. Characterization of these structures by Auger electron spectroscopy shows that the Pt areas are relatively rich in C, whereas the Sn is relatively rich in O, before and after exposure to aqueous solutions containing the organic fuel. After 3−5 min of use in 0.5 M H_2SO_4/MeOH, at potentials at which fuel oxidation occurs, redistribution of Sn to the Pt regions was observed. Sn redistribution on the time scale of the experiments is inhibited by capping the Sn with a Pt layer. In samples with capped Sn squares, the length of the Pt−Sn contact line was varied by changing the size of the structures while the exposed area of the electrode was kept constant. The activity of the capped Pt−Sn structures depends linearly on the Pt−Sn contact edge length. Thus, it is possible to confine the catalytic area of Pt−Sn electrodes by working with the appropriate structure design. The catalytic area of microfabricated Pt−Sn is located in the zone of intimate contact between the Pt and the Sn layers.

Introduction

Low-temperature fuel cells are already on the market as a highly efficient and environmentally friendly power technology option. The primary anodic fuel in such fuel cells is H_2. Unfortunately, H_2 poses dangers that lead to critical safety issues related to its generation, handling, and storage. For example, H_2 is highly flammable, and it ignites over a wider range of concentrations in air than does gasoline.[1,2] Storage is complicated by its low density under normal conditions, and it needs considerable excess weight compared to liquid fuels. Practical fuel cell applications have required that H_2 or H_2-rich gas be generated in the cell by re-forming a precursor fuel. The catalytic re-former adds weight and volume to the system and typically requires large amounts of expensive catalytic material.

Problems with H_2 have spawned great interest in the identification of possible alternative fuels. Obvious fuel requirements are availability, high energy density, low toxicity, and facility to store and handle safely. Many carbohydrates comply with such characteristics. Small organic molecules such as methanol and ethanol can be thermodynamically oxidized at potentials very close to that of H_2, which means that cell voltages obtained by coupling their oxidation to O_2 reduction should, theoretically, be close to that of the conventional H_2-O_2 fuel cell.[3] The main problem associated with the use of this type of fuel is the lack of catalyst that will oxidize hydrocarbons or even carbohydrates at useful rates and voltages.

We have previously shown that electrocodeposited Pt−Sn electrodes are good catalysts for the oxidation of several small carbohydrates such as ethanol, formaldehyde, and formic acid.[4−7] We have been interested in expanding our electrode preparation techniques to include reproducible methods for obtaining catalysts of simple and well-defined structure and composition with the goal of studying Pt−Sn interactions. Here we demonstrate microfabrication technology as a means for preparing Pt−Sn catalysts having such attributes. Such Pt−Sn surfaces contain micrometer-sized features that are easily characterized before and after use in an electrochemical cell.

Microfabrication technology has evolved to allow very large scale integration of electrical circuits (>10^6 components per chip). Recently, there has been rising interest in the use of microfabrication techniques and processes to develop micrometer-sized actuators and sensors.[8−13] Earlier work demonstrated the fabrication of microelectrochemical sensors based on the derivatization of microelectrodes with redox active molecules, conducting polymers, or metal oxides.[14−22] The main advantages derived from microelectronics fabrication in physical and chemical sensor preparation include reduced size, reduced cost, reduced sample volume, and fast response.

The ability to prepare an array of very small, identical features that are geometrically defined may also be very relevant for applications in the area of catalysis. Miniaturization of catalyst units via microfabrication should permit the enlargement and maximization of the effective surface area of a given catalytic material with very precise control of the structure and composition of such units. Also, the process can be designed so that minimal amounts of the catalytic material, which can be rare or expensive, are used during fabrication.

Microfabrication has previously been used to make heterogeneous catalysts for gaseous hydrogenation reactions. Ni catalysts composed of nanometer by micrometer metal strips separated by nanometer-thick substrate layers have been prepared by microfabrication.[23] The behavior of these catalysts was

* Address correspondence to this author at the Office of the Chancellor, Campus Box 1192, Washington University, St. Louis, MO 63130 (e-mail wrighton@wustl.edu).

[†] Motorola, Clinical Micro Sensors, 126 W. Del Mar, Pasadena, CA 91105.

[‡] Osram Sylvania Inc., Lighting Research Center, 71 Cherry Hill Dr., Beverly, MA 01010.

10.1021/jp0045336 CCC: $20.00
Published on Web 05/18/2001

similar to that of conventional supported clusters: the rate for the hydrogenolysis of ethane exhibited a maximum as a function of the Ni strip thickness, whereas no size dependency was detected for the hydrogenation of ethylene. Similarly, microfabricated structures of Pd/SiO_2 or Pd/Au have been used for the hydrogenation of 1,3-butadiene.[24−26] More recently, microfabricated Pt/CeOx catalysts were used for the oxidation of CO.[27] These works demonstrated the use of microfabrication to control the thickness, size, and spacing of catalyst and support layers.

In this paper, we illustrate the synthesis of electrochemical catalysts by microfabrication. We show that it is possible to prepare catalytically active, micrometer-sized features onto an electrode. All components of the catalyst system need to be conducting in order to have electronic access to the catalyst units. We evaluated the activity of Pt−Sn structures fabricated onto Pt toward the electrochemical oxidation of formaldehyde in 0.5 M H_2SO_4 and characterized Sn and Pt−Sn structures by Auger electron spectroscopy, atomic force microscopy, and scanning electron microscopy.

Experimental Section

Electrode Fabrication. Electrode fabrication was accomplished at the Microsystems Technology Laboratory and the Center for Materials Science and Engineering Microfabrication Facility at MIT. The methodology used for preparing the catalysts is similar to that reported previously for the fabrication of microelectrode arrays.[18,29,30] However, for this particular application, we have used the *image reversal* process, a microfabrication technique that is more compatible with the need of generating metallic layers with vertical wall profiles that are free of photoresist residues.

The direct photolithography process previously used in our laboratory produces a resist profile that is slightly trapezoidal, with positive wall slopes. As a result of the lift-off process, the first layer deposited will cover, at least to some extent, the outside vertical surface of the patterned features. Also, because of the positive wall slopes, the photoresist that has been heated upon contact with the metal being deposited can remain beneath the metallic layers after lift-off. Thus, fabrication of structures with clean edges will become particularly difficult. Image reversal, on the other hand, allows the printing of a mask in inverted tone.[28] In a first exposure, a latent image with positive wall slope is generated. Then, reversal is accomplished by a baking step followed by flood exposure. By setting the appropriate processing and developing conditions, the walls of the resist in the developed image can be tailored to have a negative slope. The undercut images are ideal for additive metallization processes.

The image reversal process for electrode fabrication is depicted in Scheme 1. The substrates were treated with hexamethyl disilazane (HMDS; used as photoresist adhesion promoter) and then coated with a 0.2-μm-thick photoresist layer. After baking at 90 °C for 30 min, the samples were exposed to UV light for 2−3 s in a Karl Suss contact mask aligner through the appropriate mask and then baked again for 90 s at 120 °C. A second exposure was accomplished through a clear mask (flood exposure) for 90 s, and then the pattern was developed for 2.5 min. Finally, the wafers were rinsed with deionized H_2O and spin-dried. The masks used in the photolithographic process were designed using the KIC program running on a Tektronics 4125 workstation. Design files were transferred electronically in the .MANN format to a GYREX e^- beam mask pattern generator run by an operator at the MIT Microsystems Technology Laboratory mask fabrication facility. All contact masks were made of chromium on glass.

SCHEME 1: Image Reversal Process for Fabrication of Sn Structures on Pt

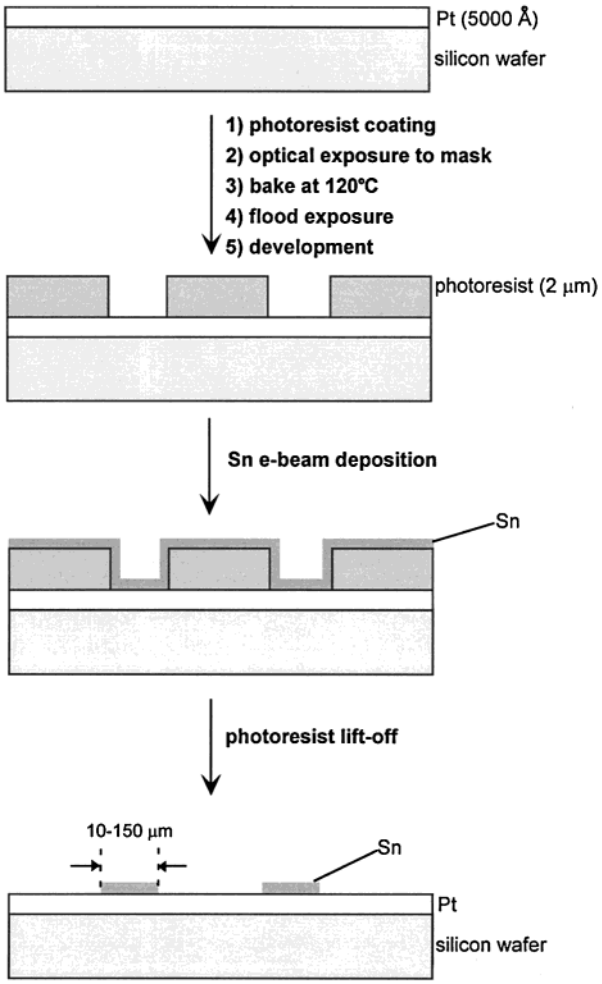

Metallization was performed in a Sloan multiple-hearth evaporator with a quartz thickness monitor, operating at $\sim 10^{-7}$−10^{-6} Torr. Sn or Sn and Pt layers were ultimately e^--beam-deposited on top of the photopatterned wafers after doing a 30-s oxygen plasma cleaning of the photoresist. The Sn layers were typically 100−300 Å thick, whereas the Pt overlayers were 300−1000 Å thick. A thin (50−100 Å) layer of Ti was always deposited prior to Sn deposition to improve Sn adhesion to Pt or to separate one layer from the other. In cases of Pt deposition onto Sn, no Ti adhesion layer was deposited. Lift-off was achieved by sonication in acetone for 2−20 min, depending on the number of metal layers deposited. Control of metal deposition temperatures was crucial, because the photoresist hardens at temperatures >100 °C and photoresist lift-off from the edges of the Pt−Sn squares or circles becomes particularly difficult to accomplish. The samples were inspected through an optical microscope after lift-off.

The process was completed by rinsing thoroughly with H_2O and spin-drying the samples. The wafers were diced by hand with a diamond scriber, and the sample pieces were divided by carefully snapping the substrates. The samples were finally rinsed in EtOH and then blow-dried with Ar before the electrochemical experiments were performed.

Electrochemistry. Electrochemical experiments were run using a PINE model RDE 4 bipotentiostat and potential programmer. Current−voltage and current−time curves were

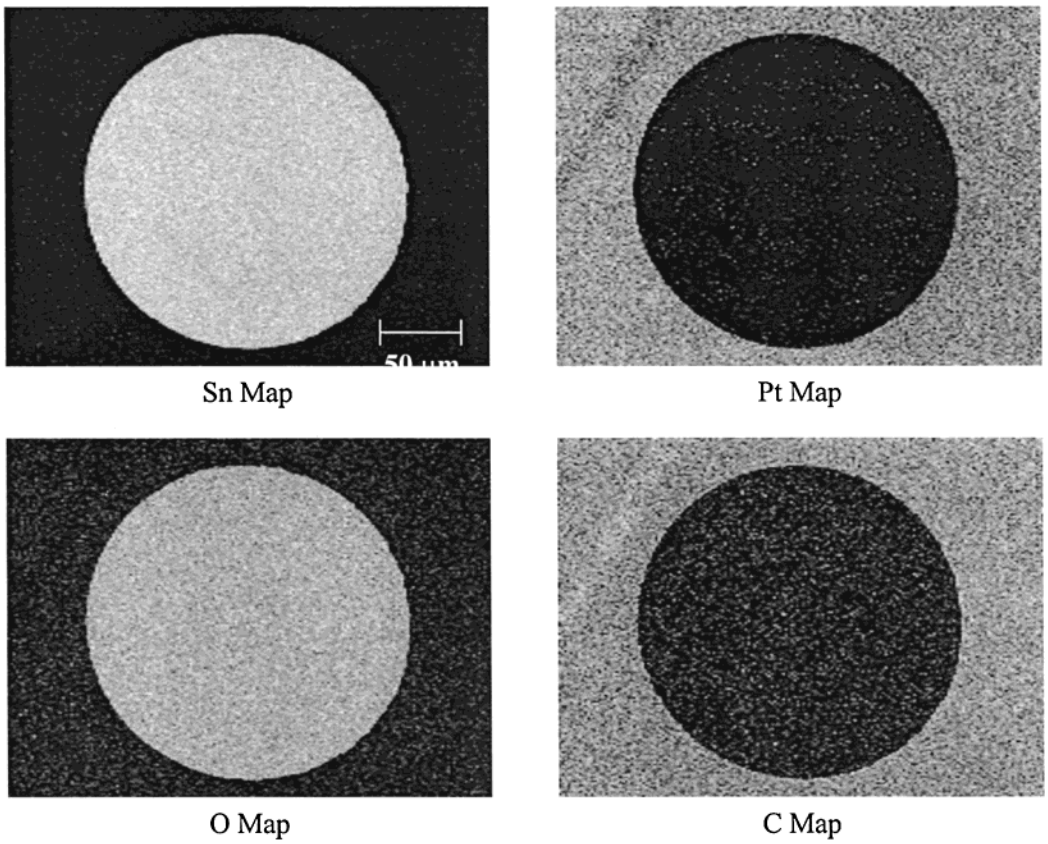

Figure 1. Pt, Sn, O, and C Auger maps of a 200-μm-diameter Sn circle on Pt. The Sn layer is 300 Å thick.

recorded on a Kipp and Zonen 90B XY or XYY′ recorder. Solutions were degassed with Ar before the experiments were run. Cyclic voltammetry was done in a one-compartment Teflon cell using a Pt gauze counter electrode and a saturated calomel reference electrode (SCE) attached to a glass Luggin capillary. The working electrodes were exposed to solution through an O-ring-sealed opening at the bottom of the Teflon cell. The area exposed was fixed and determined by the size of the O-ring ($A = 0.2827$ cm^2). Contact was made by attaching the contacting clip directly to the edge of the working electrode. Samples for Auger analysis were rinsed in H_2O and dried with Ar after the electrochemical experiment was performed, before they were introduced into the Auger chamber.

Materials. The substrates for electrode fabrication were 4-in. single-crystal Si wafers modified first with 5000 Å of thermally grown oxide and then with 1500 Å of LPCVD silicon nitride and finally coated with a 0.1−0.2-μm-thick e$^-$-beam-evaporated Pt with a Ti (100 Å) adhesion layer. The photoresist used was a Hoescht-Celanese AZ 5214 E, and the photoresist developer was a Hoescht-Celanese AZ 422 MIF. H_2SO_4 (Mallinckrodt) and HPLC grade H_2O (Omnisolve, EM Science) were used as received for the electrochemical experiments.

Surface Analysis. SEM was done on a Hitachi model S-800 electron microscope. Auger analysis was done using a Perkin-Elmer PHI 660 scanning Auger microprobe. In some cases, Ar^+ sputtering was used to remove superficial layers on the samples. Atomic force microscopy was done using a Digital Instruments Multimode with a Nanoscope III controller.

Results and Discussion

In previous work, we prepared Pt−Sn catalysts by electrocodeposition. In these catalysts, we detected a segregated Pt phase by powder XRD, but it was not possible to determine whether Sn was a segregated phase or if it was present as alloyed Sn with Pt underneath a superficial layer of Sn oxide and Pt(0).[7] We have prepared microfabricated Sn structures on Pt and used these samples as model catalysts to study Pt−Sn interactions. Figure 1 shows Auger maps of "as prepared" microfabricated Sn circles on Pt. The maps display both structural and compositional information of a particular microstructure in the finished array: the bright area corresponds in each case to the region that is rich in the element being mapped. The Sn circles are 200 μm in diameter, and the distance between them is also 200 μm. The thickness of the Sn layer is 300 Å.

The O map shows that the Sn areas are relatively rich in O vs the Pt areas. In electrodeposited Pt−Sn, although Sn is present in an oxidized state at the surface, it is mostly reduced underneath the surface layers, whereas Pt is reduced both at the surface and in the bulk.[7] This greater affinity for O of the electrodeposited or e$^-$-beamed Sn relative to Pt plays an extremely important role in the catalysis: an O source is needed to accomplish oxidation of C−H-containing molecules. Interestingly, the C map shows that the Sn regions are poor in C relative to Pt. This was also observed for samples that had been previously immersed momentarily in an aqueous solution containing the organic fuel (20% MeOH, formaldehyde, or formic acid in 0.5 M H_2SO_4) at potentials close to 0.0 V vs SCE ($-0.1 < E < +0.1$ V). Recently, it was shown that the strength of adsorption of C-containing molecules (specifically cyclohexene and CO) onto Pt−Sn surface alloys in high vacuum is also lower than for bare Pt.[31]

Adsorption of the substrate (C-containing molecule) onto the catalyst, which in microfabricated Pt−Sn occurs preferentially onto Pt regions as we have shown through the Auger data, is one more requirement for the enhancement of the rate of electrochemical oxidation of organic molecules. Still, a com-

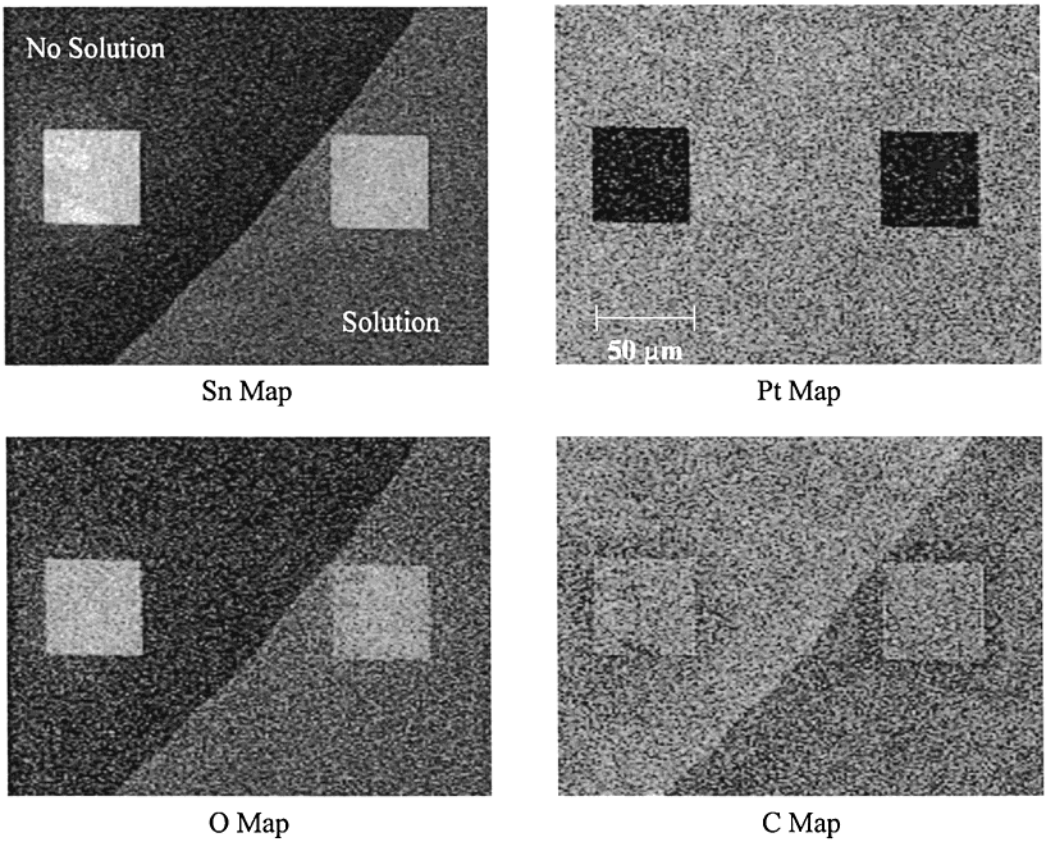

Figure 2. Sn, Pt, O, and C Auger maps of 50-μm Sn squares on Pt. The sample was partially exposed to 20% MeOH/0.5 M H_2SO_4 for 1 h at 0.0 V vs SCE, and the line of immersion is visible in the mapped area. The thickness of the Sn layer is 300 Å.

promise between organic adsorption and O adsorption *at low potentials* (E < 0.1 V) is probably achieved at Pt−Sn surfaces and not at bare Pt. At these potentials, at which the O coverage on bare Pt would be minimal, oxidation of the organic substrate will be accomplished more readily at Pt−Sn because the O coverage is increased by the presence of an oxygen source such as Sn.

Sn dissolution was observed upon prolonged immersion in solution of aqueous acid containing the organic fuel. Figure 2 shows a sample that was exposed to 20% MeOH/0.5 M H_2SO_4 for 1 h at 0.0 V vs SCE. The sample consists of 50-μm-wide and 300-Å-thick Sn squares on Pt, separated by 100 μm. The Auger maps were recorded in a region that contains the immersion line: the zone to the left side of the micrographs was kept outside the solution while the electrochemical experiment was performed. Remarkably, the Sn signal demarcates the immersed zone; that is, in the area of the sample that was exposed to solution, Sn is present not only on the squares but also on the Pt substrate.

This phenomenon of Sn redistribution was observed at potentials more negative than 0.2 V vs SCE, *where fuel oxidation is occurring.* Therefore, it is likely that Sn is competing with the organic fuel molecules for adsorption onto the Pt substrate at these potentials. It could also be competing with mildly adsorbed poison molecules: Sn might preserve Pt surfaces from irreversible adsorption of oxidation intermediates; that is, Sn might be inhibiting poison formation. Actually, the carbon map in Figure 2 shows that catalyst regions where Sn redistribution has occurred appear "cleaner" (in C species) than those that were not exposed to the solution of fuel.

Enrichment of Sn on Pt-containing surfaces has been observed by others in high vacuum by exposing Pt−Sn alloys to high temperature or an oxygen atmosphere.[32−35] Pt−Sn alloys, particularly Pt_3Sn, have been extensively studied in high vacuum for the purpose of understanding the catalysis of hydrocarbon re-forming by Pt−Sn systems supported on alumina.[32,33,35−41] The mechanism for surface Sn enrichment in Pt_3Sn (Sn segregation to the Pt-rich surface) is probably different from that of Sn enrichment of Pt backgrounds in our microfabricated Pt−Sn. However, Sn readsorption onto Pt upon exposure of microfabricated catalysts to aqueous acid is probably also related to the lower surface energy of Sn relative to Pt.[41,42]

Sn adatoms have long been known to inhibit H adsorption onto Pt, thus suppressing the hydride adsorption waves in the Pt cyclic voltammogram in aqueous acid.[43−45] In our catalysts, the Sn source is Sn(0) from the bulk of the electrodeposited electrodes or from the Sn structures in the microfabricated samples. However, inhibition of H or organic adsorption onto Pt is presumably accomplished by oxidized Sn, because redistribution of Sn to Pt background regions in the microfabricated catalysts is accompanied by a dramatic increase in the O signal on these regions in the Auger analysis (Figure 2), and Sn is present in an oxidized state at the surface of the electrodeposited catalysts, as determined by XPS.[7] Although Sn(0) is present in both types of catalysts, its influence in the adsorption stages of the electro-oxidation mechanism is probably small compared to the action of oxidized Sn, which is the only Sn species at the surface.

Figure 3 shows an AFM picture of a 20-μm-wide Pt−Sn structure on Pt. This sample was prepared by successive deposition of 300 Å Sn and 1000 Å Pt on top of a Ti adhesion layer prior to photoresist lift-off. In these structures, Sn migration is inhibited by capping the Sn with the Pt layer: after 1 day of exposure to aqueous acid, no Sn was detected on the Pt regions by Auger. A comparison of the cyclic voltammogram in 20% formaldehyde/H_2SO_4 for these structures vs bare Pt is shown

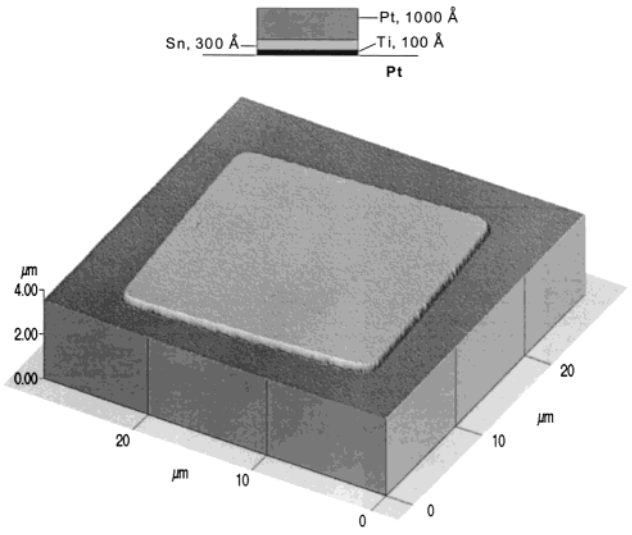

Figure 3. AFM picture of a Pt−Sn structure on Pt. The structure's width is 20 μm, and its height is 1400 Å. The Sn layer is 300 Å thick. A 100-Å layer of Ti was deposited for improvement of Sn adhesion on Pt.

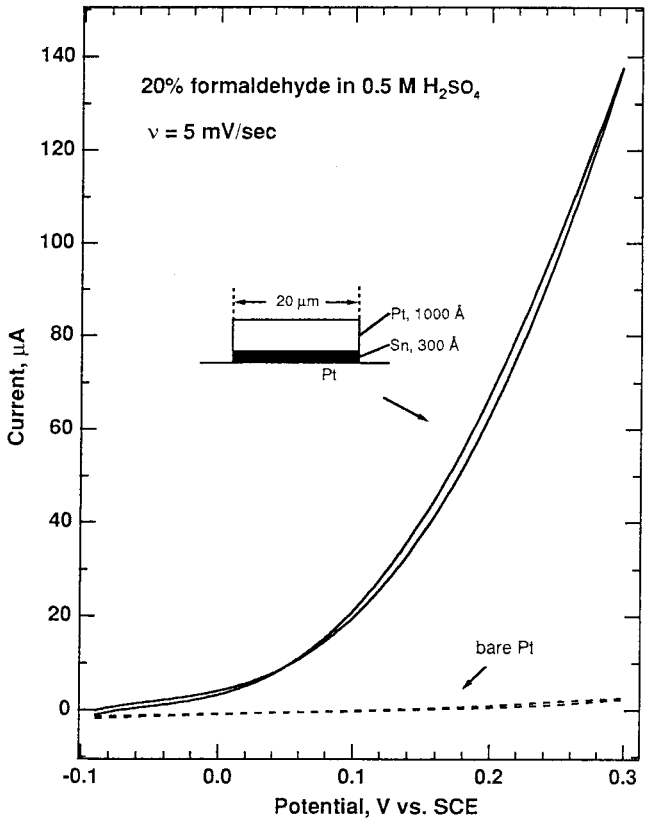

Figure 4. Cyclic voltammogram of an electrode modified by microfabrication with 20-μm-wide, 40 μm apart Pt−Sn structures on Pt in 20% formaldehyde/0.5 M H_2SO_4. The Sn layer is 300 Å thick, and the topmost Pt layer is 1000 Å thick. For comparison, a cyclic voltammogram of a bare Pt electrode in the same medium is also included. The total electrode area exposed was 0.2827 cm^2 in both cases, and the sweep rate was 5 mV/s.

in Figure 4. The onset for oxidation current at the microfabricated Pt−Sn is ~200 mV more negative than for bare Pt, and there is a 10-fold increase of the current at 0.05 V vs SCE. There is very small hysteresis in the cyclic voltammogram for the microfabricated electrode, which suggests that there was little change of the catalytic surface while formaldehyde was oxidized in either direction of the potential sweep.

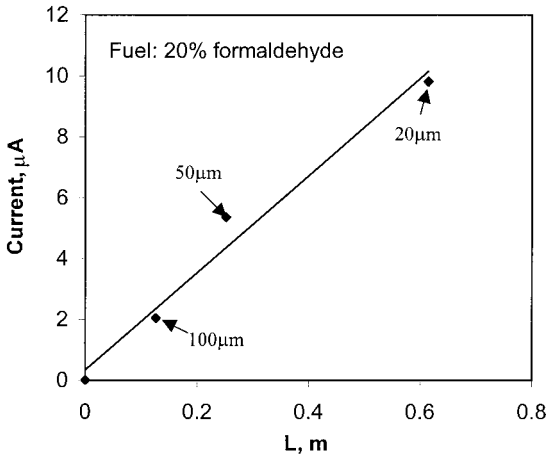

Figure 5. Plot of the current at E = 0.05 V vs SCE in 20% formaldehyde/0.5 M H_2SO_4 vs Pt−Sn contact length. L is the total number of squares in the electrode area exposed to solution times the perimeter of each square. Each point represents the current recorded at 0.05 V for a sample that contains structures having widths indicated in the plot.

Cleanliness of the edges of the Pt−Sn structures was crucial for the detection of excess catalytic activity with respect to the Pt electrode of the same area. No Sn redistribution was observed for these samples, so we are certain that the excess current is being produced at the edges of the squares. Confinement of the catalytic area is an appealing feature of microfabrication as a tool for catalyst preparation because it allows control of the activity by design of the structure shape, size, and number in a catalyst array. These are variables that can be easily predetermined by using the appropriate mask in the exposure step of the fabrication. Moreover, the composition of the structures can also be tailored to tune the catalytic activity according to the fuel to be oxidized.

We prepared several catalyst arrays with Pt−Sn squares of different sizes: 100-, 50-, and 20-μm-wide squares. By varying the structure size we could change the structure population in the catalyst array while keeping the Pt area and the total electrode area constants. Thus, only the total edge length was different from one sample to the other. Figure 5 shows a plot of the current vs the edge length (L = total number of squares × perimeter of each square) at 0.050 V vs SCE. The linear dependence of the current with L confirms that the catalytic area is located in the region of intimate contact between Pt and Sn at the edges of the squares.

It is also possible to increase the edge length by adding Pt−Sn layers to the array, that is, by building up towers that grow in the direction perpendicular to the plane of the wafer (substrate). We prepared 100-, 50-, and 20-μm-wide towers by depositing two sets of Pt−Sn layers separated by a layer of Ti (100 Å thick). The Pt−Sn contact length in these structures is twice the contact length in the array that contains just one set of Pt−Sn layers of the same structure size. Figure 6 shows an SEM micrograph of the edge of one of the 100-μm-wide towers.

The slope of the current vs Pt−Sn contact length plot (2[Pt−Sn]) is twice the slope of the current vs Pt−Sn edge length plot (1[Pt−Sn]) (Figure 7). This means that, for the same structure size, the current increases in a 4-fold fashion by adding a second layer of Pt−Sn. As we are measuring the rate of the same reaction, the slope should be the same for both plots. The discrepancy is likely to be due to the interdiffusion of Sn through the edge width. If this is true, and the Sn interdiffusion region has the same width for the two-layered and the four-layered Pt−Sn towers, a plot of the current vs the edge area should be

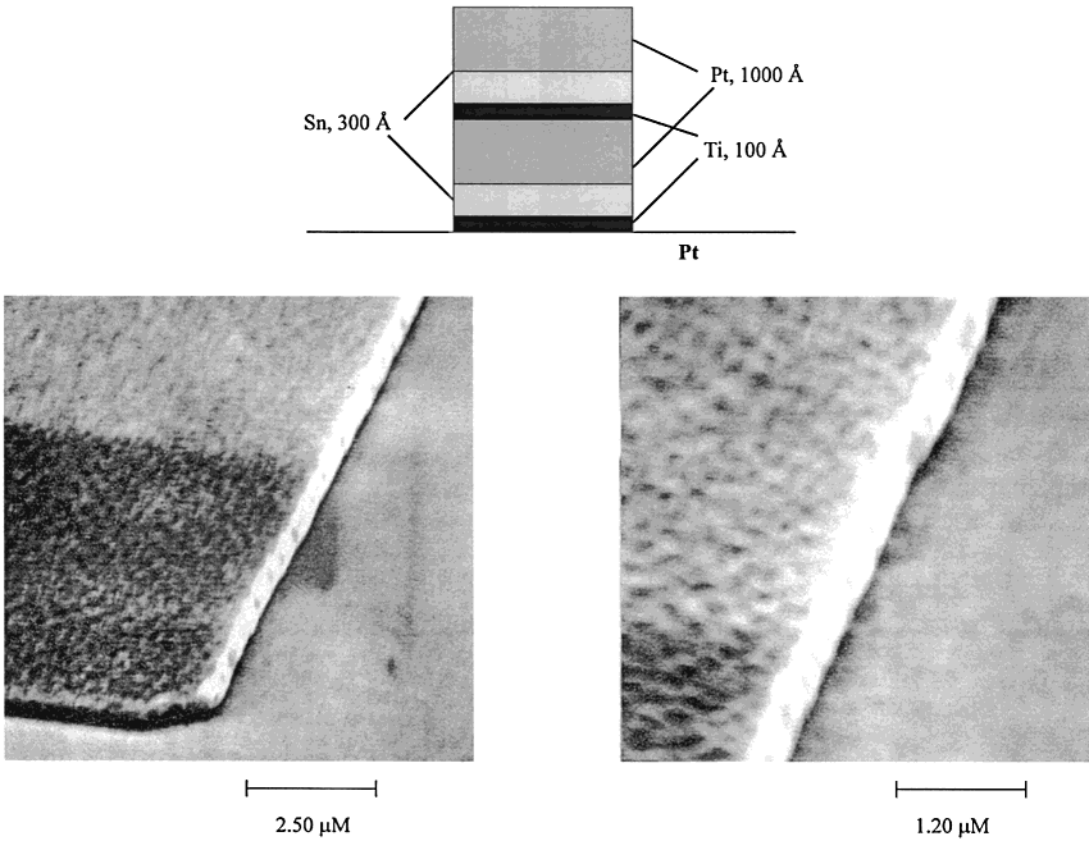

Figure 6. SEM micrographs showing the edge of a 100-μm-wide structure that contains two Pt−Sn bilayers separated by a 100-Å Ti layer. The Sn layers are 300 Å thick, and the Pt layers are 1000 Å thick.

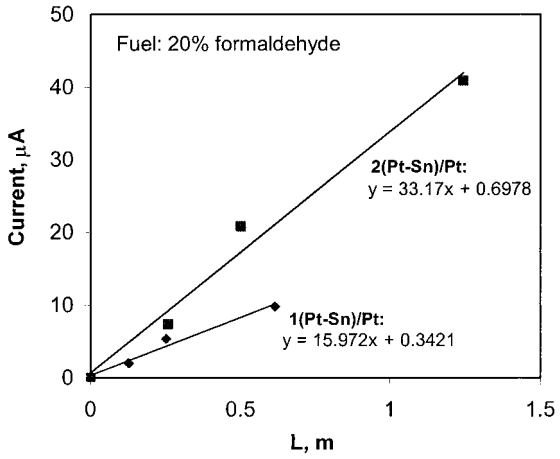

Figure 7. Plot of the current at E = 0.05 V vs SCE in 20% formaldehyde/0.5 M H_2SO_4 as a function of the Pt−Sn contact length for samples that contain one and two sets of Pt−Sn layers. L is the total number of squares times the perimeter of each square in the case of one Pt−Sn bilayer and the total number of squares times twice the perimeter of each square for the samples with two Pt−Sn bilayers.

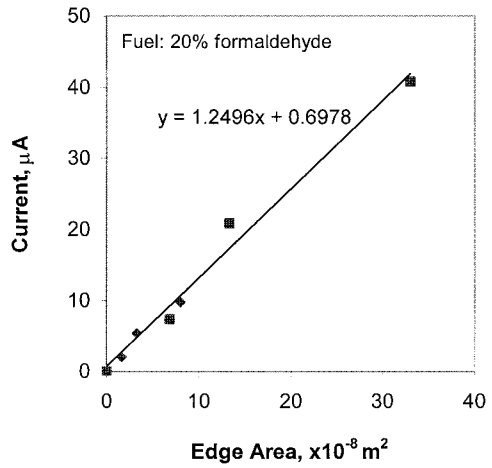

Figure 8. Plot of the current at E = 0.05 V vs SCE in 20% formaldehyde/0.5 M H_2SO_4 vs total edge area for samples that contain one and two sets of Pt−Sn layers.

linear and it should comprise all the points (for both types of samples). We show this plot in Figure 8. We assume that the Sn diffuses through the whole column edge, but this is not necessarily true. The important result is that, when we account for both the increase in edge area and the increase in catalytic material, we obtain the expected dependence of the current with the total amount of Pt−Sn contact strips.

Conclusions

We have prepared microfabricated Sn structures on Pt and used these samples as model catalysts for the oxidation of small organic fuels (MeOH, formaldehyde, and formic acid). Auger analysis of these structures shows that the Pt areas are relatively rich in C, whereas the Sn is relatively rich in O, before and after exposure to aqueous solutions containing the organic fuel. At low potentials (E < +0.1 V), where the O coverage on bare Pt is minimal, Sn behaves as an oxygen source for oxidation of the organic fuel.

Upon immersion for longer times (~0.5 h or more) in aqueous solutions of the fuel, Sn redistribution to the Pt substrate is observed at potentials at which fuel oxidation occurs (−0.1 to +0.1 V vs SCE). Sn dissolution and readsorption can be inhibited by capping the Sn with a Pt layer. For the Pt-capped Sn structures, the oxidation currents are mostly generated at the edges of the structures. This was corroborated by determin-

ing the variation in activity produced by changing the size of the structures or the number of Pt−Sn layers while keeping the exposed area of the electrode constant. We showed that the activity of the capped Pt−Sn structures depends linearly on the Pt−Sn contact edge length. Thus, we have been able to confine the catalytic area of an electrode to submicrometer(nano)-sized strips (edges of squares). Catalysis on these strips is affected by interdiffusion of Sn through the strip width.

The total currents obtained from the microfabricated catalysts are much lower than those required for practical applications. However, we envision the possibility of preparing high surface area electrocatalysts by microfabrication onto nonrigid substrates. The main advantage of such systems will be that it will be feasible to design the structure, size, and composition of the catalyst unit and that fabrication will be reproducible.

Acknowledgment. We thank the Advanced Research Projects Agency for support of this research and the National Science Foundation for support of the Surface Analysis Facilities at the Center for Material Science and Engineering (MRSEC Facilities, DMR-900334). We also thank the personnel of the Microsystems Technology Laboratory and the Center for Materials Science and Engineering Microfabrication Facilities at MIT for technical assistance. M.J.G. thanks INTEVEP, the research and technological support center of Petróleos de Venezuela, for financial support.

References and Notes

(1) Appleby, A. J.; Foulkes, F. R. *Fuel Cell Handbook*; Van Nostrand Reinhold: New York, 1989.
(2) Kartha, S.; Grimes, P. *Phys. Today* **1994**, Nov, 54.
(3) Latimer, W. M. *The Oxidation State of The Elements and Their Potentials in Aqueous Solutions*, 2nd ed.; Prentice-Hall: New York, 1952.
(4) Hable, C. T.; Wrighton, M. S. *Langmuir* **1991**, *7*, 1305.
(5) Hable, C. T.; Wrighton, M. S. *Langmuir* **1993**, *9*, 3284.
(6) González, M. J.; Hable, C. T.; Wrighton, M. S. *J. Phys. Chem. B* **1998**, *102*, 9881.
(7) González, M. J.; Peters, C. H.; Wrighton, M. S. *Chem. Mater.* **2001**, submitted for publication.
(8) Wu, Q.; Lee, K.-M.; Liu, C.-C. *Sens. Actuators B* **1993**, *13*−*14*, 1.
(9) Smela, E.; Inganäs, O.; Lundström, I. *Science* **1995**, *268*, 1735.
(10) Delapierre, G. *Sen. Actuators* **1989**, *17*, 123.
(11) Liu, C. C.; Jin, Z.; Savinell, R. F. *Proc. Electrochem. Soc.* **1998**, *98-14*, 112.
(12) Liu, C. C. *Appl. Biochem. Biotechnol.* **1993**, *41*, 99.
(13) Wang, X.; Liu, C. C.; Jin, Z.; Hughes, H. G. *Proc. Electrochem. Soc.* **1997**, *97-5*, 199.
(14) Kittlesen, G. P.; White, H. S.; Wrighton, M. S. *J. Am. Chem. Soc.* **1985**, *107*, 7373.
(15) Huang, J.; Wrighton, M. S. *Anal. Chem.* **1993**, *65*, 2740.
(16) Mirkin, C. A.; Wrighton, M. S. *J. Am. Chem. Soc.* **1990**, *112*, 8596.
(17) Chao, S.; Wrighton, M. S. *J. Am. Chem. Soc.* **1987**, *109*, 6627.
(18) Kittlesen, G.; White, H.; Wrighton, M. S. *J. Am. Chem. Soc.* **1984**, *106*, 7389.
(19) Thackeray, J. W.; White, H. S.; Wrighton, M. S. *J. Phys. Chem.* **1985**, *89*, 5133.
(20) Schloh, M. O.; Leventis, N.; Wrighton, M. S. *J. Appl. Phys.* **1989**, *66*, 965.
(21) Natan, M. J.; Wrighton, M. S. In *Progress in Inorganic Chemistry*; Lippard, S. J., Ed.; Wiley: New York, 1989; Vol. 37, p 391.
(22) Mirkin, C. A.; Valentine, J. R.; Ofer, D.; Hickman, J. J.; Wrighton, M. S. In *Biosensors and Chemical Sensors*; Edelman, P. G., Wang, J., Eds.; ACS Symposium Series 487; American Chemical Society: Washington, DC, 1992; p 218.
(23) Zuburtikudis, I.; Saltsburg, H. *Science* **1992**, *258*, 1337.
(24) Krauth, A. C.; Lee, K. H.; Bernstein, G. H.; Wolf, E. E. *Catal. Lett.* **1994**, *27*, 43.
(25) Krauth, A. C.; Bernstein, G. H.; Wolf, E. E. *Catal. Lett.* **1997**, *45*, 177.
(26) Wolf, E. E. *Top. Catal.* **2000**, *13*, 21.
(27) Johansson, S.; Fridell, E.; Kasemo, B. *J. Vac. Sci. Technol. A***2000**, *18*, 1514.
(28) Willson, C. G. *Introduction to Microlithography*, 2nd ed.; Thompson, L. F., Willson, C. G., Bowden, M. J., Eds.; American Chemical Society: Washington, DC, 1994.
(29) Paul, E. W.; Ricco, A. J.; Wrighton, M. S. *J. Phys. Chem.* **1985**, *89*, 1441.
(30) White, H. S.; Kittlesen, G. P.; Wrighton, M. S. *J. Am. Chem. Soc.* **1984**, *106*, 5375.
(31) Xu, C.; Koel, B. E. *Surf. Sci. Lett.* **1994**, *304*, L505.
(32) Hoflund, G. B.; Asbury, D. A.; Kirszensztejn, P.; Laitinen, H. A. *Surf. Sci.* **1985**, *161*, L583.
(33) Hoflund, G. B.; Asbury, D. A. *Langmuir* **1986**, *2*, 695.
(34) Hoflund, G. B.; Asbury, D. A.; Kirszensztejn, P.; Laitinen, H. A. *J. Interface Anal.* **1986**, *9*, 169.
(35) Asbury, D. A.; Hoflund, G. B. *Surf. Sci.* **1988**, *199*, 552.
(36) van Santen, R.; Sachtler, W. *J. Catal.* **1974**, *33*, 202.
(37) Biloen, P.; Bouwman, R.; van Santen, R.; Brongersma, H. *Appl. Surf. Sci.* **1979**, *2*, 532.
(38) Bouwman, R.; Biloen, P. *Surf. Sci.* **1974**, *41*, 348.
(39) Bouwman, R.; Toneman, L. H.; Holscher, A. A. *Surf. Sci.* **1973**, *35*, 8.
(40) Gardner, S. D.; Hoflund, G. B.; Schryer, D. R. *J. Catal.* **1989**, *119*, 179.
(41) Haner, A. N.; Ross, P. N.; Bardi, U. *Surf. Sci.* **1991**, *249*, 15.
(42) Paffett, M. T.; Logan, A. D.; Simonson, R. J.; Koel, B. E. *Surf. Sci.* **1991**, *250*, 123.
(43) Szabó, S. *J. Electroanal. Chem.* **1984**, *172*, 359.
(44) Stefenel, M. M.; Chierchie, T.; Mayer, C. *Z. Phys. Chem. Neue Folge* **1983**, *135*, 251.
(45) Janssen, M. M.; Moolhuysen, J. *J. Catal.* **1977**, *46*, 289.